Using the X-shooter physical model to understand instrument flexure

Paul Bristow[a], Joel Vernet[a], Florian Kerber[a] Sabine Moehler[a], Andrea Modigliani[a]

[a]ESO - ESO, Karl-Schwarzschild-Str. 2, 85748 Garching, Germany;

ABSTRACT

We have developed a physical model of the VLT 2nd generation instrument X-shooter. The parameters of this model, that describe the positions, orientations and other physical properties of the optical components in the spectrograph, are continually updated by an optimisation process that ensures the best possible fit to arc lamp line positions in calibration exposures. Besides its use in driving the wavelength calibration in the data reduction pipeline, the physical model provides us with an insight into physical changes in the optical components and the possibility to correlate these with changing instrument orientation. By utilising a continually growing database of automatic flexure compensation exposures that cover a wide range of instrument orientations, we are able to investigate flexure in terms of physical model parameters.

Keywords: Spectroscopy, Wavelength Calibration, Instrument Modelling, Flexure

1. INTRODUCTION

X-shooter[1] is a single target spectrograph mounted at the Cassegrain focus of VLT UT2 covering in a single exposure the spectral range from the UV to the K band (300 -2500 nm). It is designed to maximize the sensitivity in this spectral range by splitting the incoming light into three arms (UVB, VIS and NIR) with optimized optics, coatings, dispersive elements and detectors, operating at intermediate resolutions (R=4000-14000). Each of the three arms constitutes an echelle spectrograph with cross dispersion achieved through a prism (or multiple prisms in the case of NIR) in double pass and principle dispersion via a diffraction grating.[2] X-shooter achieved first light (all three arms together) in March 2009 and has been available to the community since October 2009.

Data reduction for X-shooter is supported by a full featured data reduction software[3] (hereafter DRS) which includes a physical model[5,4] (hereafter XSPM; see section 2) of the principal dispersive elements of each of the spectrographs to drive the wavelength calibration. During routine operations the parameters of the XSPM are regularly optimised to ensure the best match to calibration exposures. ESO quality control (QC) archives and monitors these parameters along with other diagnostics describing the changing operational environment. In a separate paper[6] we discuss what can be learnt from the QC data set. Here we concentrate on the variation of XSPM parameters with instrument orientation in order to better understand flexure.

Figure 1 shows X-shooter mounted at the Cassegrain focus of VLT UT2. The UVB and VIS spectrographs can be seen at the sides, whilst the NIR spectrograph resides in the dewar visible at the base. Clearly the orientation of the spectrographs will vary with the zenith angle and, away from the zenith, with the position angle. It is known that flexure causes the source to move on the spectrograph entrance slits (which is ameliorated by an active flexure compensation system) and some movement of the spectrograph optical components. The latter effect is corrected to first order in the DRS pipeline, we use the physical model to investigate the physical interpretation of the spectrograph flexure and to characterise higher order components.

2. THE X-SHOOTER PHYSICAL MODEL

2.1 Model Structure

The X-shooter optical model has a model kernel that is a fast, simplified ray trace code. The speed with which the streamlined model can be evaluated makes it suitable for iterative evaluation for many different wavelengths

Further author information: (Send correspondence to Paul Bristow)
Paul Bristow: E-mail: bristowp@eso.org, Telephone: +49 89 32006454

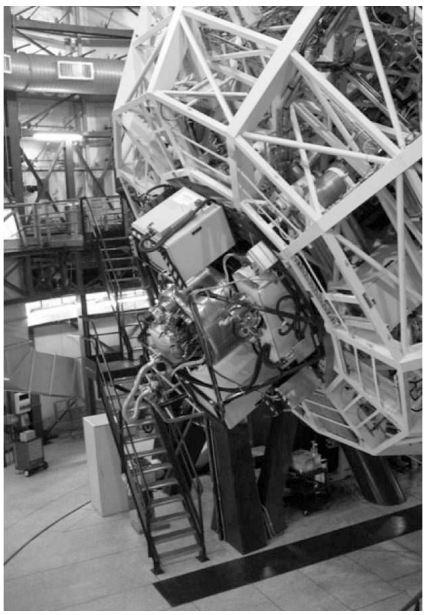

Figure 1. X-shooter mounted on the Cassegrain focus of UT2.

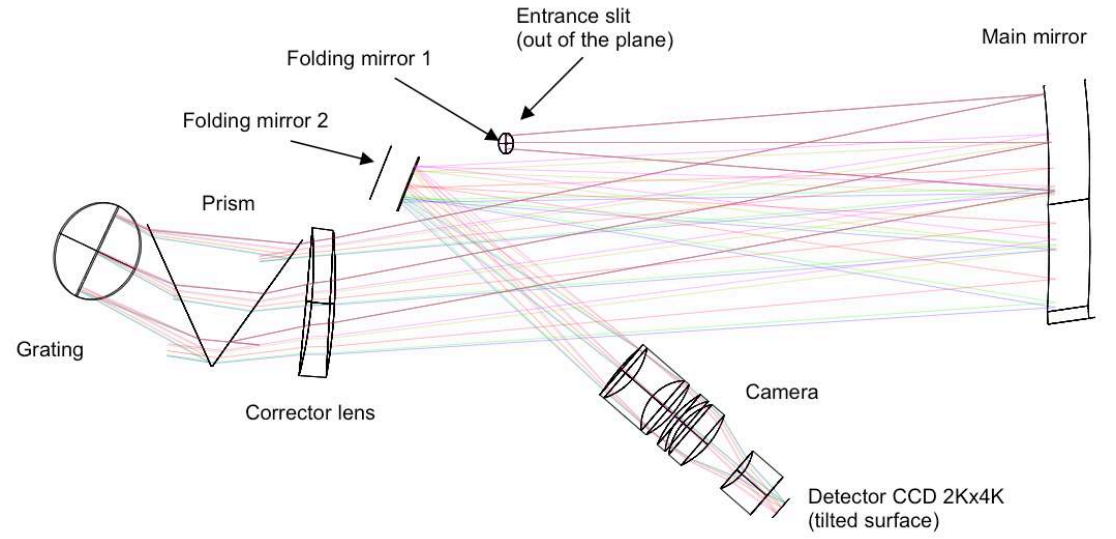

Figure 2. The optical layout of the X-shooter UVB arm, reproduced from the X-shooter Optical Design Report[2] . The VIS arm is qualitatively the same whilst the NIR arm is similar but has two additional cross-disperser prisms.

and slit positions. Most importantly, parameters describing the configuration of the optical components can be optimized using the Monte-Carlo type "Adaptive Simulated Annealing" technique[7,8] so long as appropriate calibration data are available. Consequently we are able to fit the dispersion solution with a set of physically meaningful parameters.

Following the prescription of Ballester & Rosa (1997)[9] , the core of the X-Shooter PM is a series of matrix transformations, each representing an optical surface in the spectrograph as specified in the detailed Zemax optical design[2] . This enables determination of the location at which a ray of given wavelength and entrance slit position intersects the detector plane. The matrix transformations embody the tips and tilts of the optical components.

The optical layout of the X-shooter UVB arm is shown in figure 2 (reproduced from the X-shooter Optical Design Report[2]). The UVB and VIS arms of the X-shooter spectrograph are very similar in design and can be described by the same set of matrix transformations, they simply require distinct parameter sets. The NIR arm is also very similar, having just two additional cross-dispersion prisms, therefore we are able to use a slightly adjusted model kernel and parameter set that includes the additional prism transformations and appropriate parameters. The parameter sets for the three arms can be summarised as follows:

- Entrance slit & collimator
  - Relative position and orientation of the slit
  - Focal length of collimator
- Cross-disperser Prism(s)
  - Orientation of 1st surface μ_{p1}, ν_{p1} (The NIR arm has three cross-disperser prisms, the orientation of the initial surfaces of the 2nd and 3rd prisms are described by μ_{p3}, ν_{p3} and μ_{p5}, ν_{p5} respectively)
  - Orientation of 2nd surface μ_{p2}, ν_{p2} (for NIR also μ_{p4}, ν_{p4} and μ_{p6}, ν_{p6})
  - Temperature (obtained from exposure header)
  - Refractive index (*not* a parameter but computed from reference data as a function of wavelength and temperature.
- Reflection grating
  - Orientation μ_g, ν_g, τ_g
  - Grating constant s_g
- Camera and detector array
  - Focal length of focusing optics f_d
  - Orientation of detector μ_d, ν_d, τ_d
  - Relative position of detector X_d , Y_d
  - Dimensions of pixel grid

Also provided in the above list are the abbreviations for the parameters as used in section 5 and table 1.

Hence there is a complete set of parameters that describe the passage of a photon through the spectrograph. These parameters are physical quantities (angles, distances, temperatures etc.) and describe the actual status of components. They can be adjusted at any time to match the observed behaviour of the instrument or to predict the effects of tilting/modifying a component.

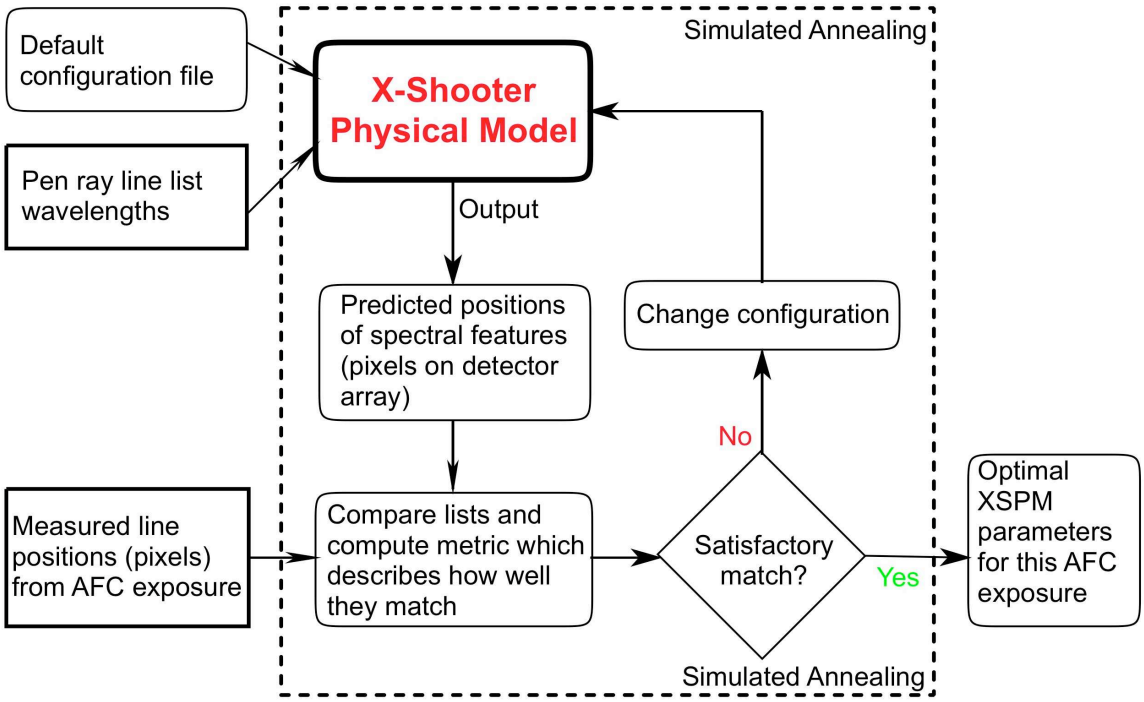

Figure 3. The optimisation process used to modify XSPM parameters to fit each AFC exposure.

2.2 Model Optimisation

In order to establish the physical parameter values that allow the XSPM to reproduce the observed performance of the spectrograph, we require a set of identified calibration features from a calibration exposure, in the analysis presented here we use the automatic flexure compensation (AFC) exposures. We then iteratively call the core model function for the identified calibration wavelengths, comparing the results of each iteration to the centroids for these wavelengths as measured in the calibration data. We employ the Taygeta[10] implementation of the simulated annealing technique[7,8] to continually adjust the model parameters until the best match between predicted and measured centroids is found. Figure 3 is a schematic representation of this procedure for the case of automatic flexure compensation exposures.

3. X-SHOOTER AUTOMATIC FLEXURE COMPENSATION

Since X-shooter is a three arm Cassegrain instrument, active flexure compensation is essential to keep the target simultaneously on all three arms,[11] describes the strategy adopted in detail. The procedure can be briefly summarised as follows:[12]

1. Take a pinhole arc-lamp calibration spectrum of each of the spectrographs alone
2. Take an arc-lamp calibration of a pinhole placed in the cassegrain focal plane with each spectrograph
3. Analyze and correct flexure: cross correlate frames taken in (1) and (2) and apply an appropriate offset to the tip-tilt tables for each arm
4. (optional) Repeat step (2) to confirm the correction

Thus a flexure compensation for the beam before it enters the spectrograph slits is dynamically applied.

However, further flexure occurs within the individual spectrographs. Fortunately the first of the sequence of exposures listed above can be used to measure the flexure this spectrograph flexure for each arm. Currently, during routine operations, the DRS uses the positions of lines measured in this exposure to determine a linear global shift to the spectral format as a first order correction to flexure in the spectrograph.

4. ANALYSIS OF AFC EXPOSURES WITH THE PHYSICAL MODEL

Using the physical model we can attempt to do better. Rather than just a first order global correction, we can re-optimise the XSPM parameters as described in section 2.2. Then we can look for correlations between the values of the optimised physical parameters and the orientation of the instrument at the time each AFC exposure was obtained (available in the ALT and POSANG header keywords). This offers the chance to understand what is happening in the instrument as it flexes. Further, if we find strong correlations then we may be able to predict what happens to some physical parameters as X-shooter rotates, allowing even the possibility that we could predict how these parameters changed during a long integration and use a parameter set in the DRS that is adjusted accordingly rather than just optimised to the AFC taken immediately before the science exposure.

Fortunately there is a plentiful supply of AFC exposures since they are taken before every science exposure. We take a large sample: 700 per arm from March and April 2010. This data set does not however allow us to investigate hysteresis which we leave outside the scope of this paper except for noting that it is an obvious source of scatter in our results.

Unfortunately, in order to reduce the read time required for these AFC exposures, only 1000pix $\times$ 1000pix sub-windows of the UVB and VIS detectors are read out. The NIR CMOS detector has a much higher read out rate and is smaller so it is possible to read out the entire array (in fact windowing was not, initially, available on this device). Moreover, the exposure times are kept very short, so the number of lines bright enough to give an accurate centroid in a given sub-window is very much lower than the number of lines available in regular wavelength calibration exposures (UVB 20 lines; VIS 14 lines; NIR 20 lines, counting wavelengths appearing in multiple orders as multiple lines).

So clearly we must be careful not to leave too many parameters open in the optimisation process, since in any given AFC exposure we have only a handful of data points. A further reason for careful selection of open parameters is that many of the XSPM parameters are degenerate to first order and data points from only a sub-window of the detector does not give much chance of breaking that degeneracy. Bearing this in mind, we adopted the approach of first optimising with a large subset of XSPM parameters open, essentially any parameter that may reasonably be affected by flexure. This will give us an idea of the minimum residuals that we can expect in any fit to this data. However, due to degeneracy between the parameters, any correlations with instrument orientation will be washed out. So we then proceed with a trial-and-error process of re-optimising with smaller groups of open parameters with the aim of discovering a smaller set of parameters that have similar residuals to the earlier results. In this way we expect to reduce our number of open parameters to a core group that can explain the movement of calibration lines due to flexure.

5. RESULTS

Table 1 shows the mean x and y residuals for the best fit achieved with various combinations of open parameters for the three spectrographs. Note that this mean is over the $N \simeq 600$ exposures and over the number of lines matched in each exposure, $M \simeq 11, 14, 20$ for UVB, VIS and NIR respectively. Moreover the mean value for each exposure is in fact the mean absolute value:

$$\bar{\Delta x} = \frac{1}{N}\sum_{i=1}^{N}\frac{1}{M}\sum_{j=1}^{M}\|\delta x_j\| \tag{1}$$

($\bar{\Delta y}$ is defined in the same way).

The first row of the table gives the results obtained with all XSPM parameters that are plausibly related to flexure open. This is a good approximation as to the minimum possible mean residuals for each arm, however

degeneracy between the parameters means that correlations between XSPM parameters and flexure are washed out in this data. By contrast the second row gives the results when only the detector zero points, X_d and Y_d, are open. These mean residuals represent what happens currently in the pipeline where a uniform shift is applied to the spectral format. Clearly the mean residuals are higher since non-linear flexure effects cannot be accounted for. Nevertheless, for a given line the flexure typically results in a maximum euclidean offset of $\gtrsim$ 1pix, (the exact value depending on the position on the detector) so the uniform shift alone removes the most significant component of flexure for all three arms.

Table 1. Mean x and y residuals resulting from various combinations of open XSPM parameters during optimisation. See section 2 for an explanation of the XSPM parameters and section 5 for the definition of $\bar{\Delta}x$.

	UVB		VIS		NIR	
Open parameters	$\bar{\Delta}x$ (pix)	$\bar{\Delta}y$ (pix)	$\bar{\Delta}x$ (pix)	$\bar{\Delta}y$ (pix)	$\bar{\Delta}x$ (pix)	$\bar{\Delta}y$ (pix)
All	0.041	0.046	0.027	0.025	0.041	0.090
X_d, Y_d	0.067	0.073	0.037	0.036	0.074	0.112
X_d, Y_d, τ_d, f_d	0.044	0.048	0.028	0.026	0.047	0.098
X_d, Y_d, τ_d, f_d, μ_g, ν_g	0.041	0.046	0.025	0.027	0.041	0.090
τ_d, f_d, μ_g, ν_g	0.041	0.046	0.027	0.028	0.043	0.096
τ_d, f_d, μ_g, ν_g, μ_d, ν_d	0.040	0.045	0.027	0.022	0.042	0.094

In most of the analysis that follows we concentrate on the NIR spectrograph since the 2nd order flexure effects appear to be stronger and the correlations in the results are clearer, probably indicating that the NIR spectrograph, with its heavy cross-disperser prisms, is more susceptible to flexure.

Figures 4 and 5 show the correlation between X_d and Y_d and the instrument orientation for the case of all parameters open and the case of only X_d and Y_d open. In figure 5 we see an obvious correlation, whereas in figure 4 this correlation is washed out due to degeneracy with other parameters. Moreover, the correlation in figure 5 is not physically satisfying in that the trend of both X_d and Y_d with sin(ALT) is in the same sense regardless of POSANG whereas one would expect the sense to change as POSANG changes by 180 degrees. In addition, the smaller mean residuals obtained with all parameters open tells us that we ought to be able to find correlations to other XSPM parameters.

We next tried to introduce parameters that would allow 2nd order effects of zoom (f_d) and rotation (τ_d). This results in reduced mean residuals (row 3), but they are still significantly higher than the all open case for NIR (the effect is smaller for the other two arms). Consequently we introduced two further parameters that allow for some non-linear offsets, μ_g, ν_g. This results in mean residuals (row 4) that are very similar to the all open case. Moreover, the camera focal length can be seen to vary in an intuitively plausible way with sin(ALT) and POSANG (this correlation was not clear in the results with all parameters open) as shown in figure 6. However, for this set of open parameters the X_d and Y_d correlation has been washed out by first order degeneracy with μ_g and ν_g, which also show some weak correlation with flexure.

So we then tried the same combination of open parameters again except with X_d and Y_d closed. The mean residuals (row 5) are once again similar to the all open case (and better than the earlier case in row 3 where X_d and Y_d replaced μ_g and ν_g). Figure 7 shows the correlation of μ_g and ν_g with flexure, while figure 8 show the correlations between f_d and orientation and τ_d and orientation for this combination of open parameters. For all four parameters there is a clear dependence upon sin(ALT) and POSANG.

Finally, we try to improve the residuals to match those in row 1 without reintroducing X_d and Y_d, instead we introduce μ_d and ν_d. This does have the desired effect on the residuals (row 6) but plots of μ_d and ν_d against orientation (figure 9) do not show any clear trends.

Therefore, for NIR we conclude that f_d and τ_d have clear dependencies upon orientation that are qualitatively consistent even when the other open parameters are changed. On the other hand, the pairs of parameters (X_d, Y_d) and (μ_g, ν_g) (and further analysis reveals that the same is true also for $(\mu_{p1,3,5}, \nu_{p1,3,5})$) show clear dependencies upon orientation but are degenerate. Our current data set does not enable us to decisively break this degeneracy.

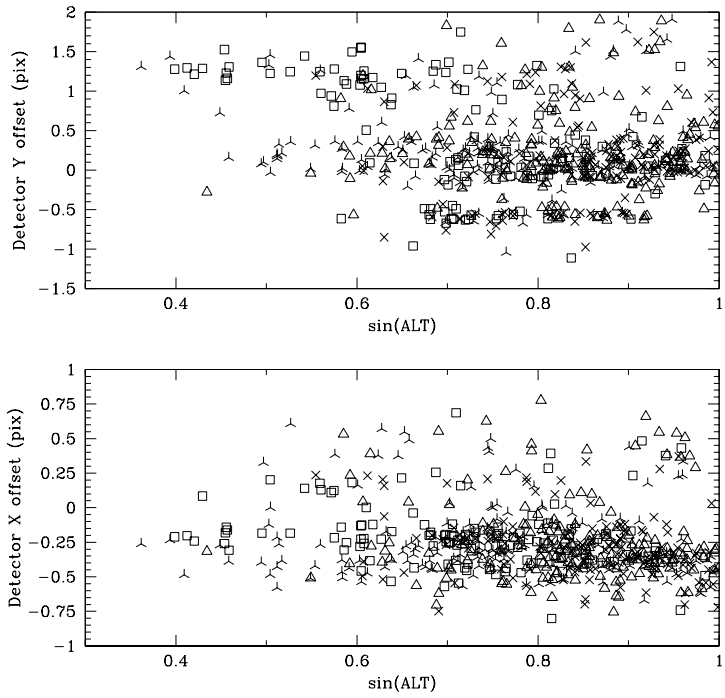

Figure 4. **Top:** The optimal value of the NIR detector x offset parameter, X_d, determined via application of the optimisation process with *all* applicable XSPM parameters open, plotted against the sin of the ALT header keyword (i.e. the vertical component, at the zenith $\sin \mathrm{ALT} = 1$). The header POSANG keyword is indicated by the symbols as follows: 3 pointed star $\Rightarrow$ POSANG$< -90^\circ$; open triangle $\Rightarrow -90^\circ \leq$POSANG$< 0^\circ$; cross $\Rightarrow 0^\circ \leq$POSANG$< 90^\circ$; open square $\Rightarrow$POSANG$> 90^\circ$. **Bottom:** The same plot for the NIR detector y offset parameter, Y_d.

We conducted similar analysis for the UVB and VIS spectrographs, but the results were less conclusive. This is to be expected since AFC exposures include the entire NIR FoV, but only 1000pix×1000pix sub-windows from UVB and VIS. Moreover, there is no reason to expect the same kind of dependencies for the UVB and VIS spectrographs since, being situated at the sides rather than the base of the Cassegrain mount (see figure 1), the geometry is different. Nevertheless there are correlations that can be identified in the UVB and VIS data as shown in figures 10 and 11. Here the open parameters were μ_g, ν_g, f_d and τ_d and we see a clear dependence of μ_g and ν_g upon orientation, though no such correlation is evident for f_d and τ_d. VIS results are qualitatively similar to UVB.

6. SUMMARY

For the X-shooter NIR arm we found correlations between XSPM parameters and instrument orientation. Whilst degeneracy between XSPM parameters leaves some uncertainty as to the exact physical interpretation, we have taken steps to isolate a small group of physically plausible parameters that provide both a good fit to the data and have a strong correlation with instrument orientation. The correlations are consistent with the flexure that might be expected due to the heavy NIR cross-disperser prisms and the heavy copper bar linked to the detector mount (laboratory testing lead to a modification of this link that reduced testing). Moreover, these correlations allow us to predict how the spectral format varies with flexure. To obtain clearer results for the UVB and VIS spectrographs it may be necessary to obtain a dedicated set of full detector read out exposures for the full range of detector orientations.

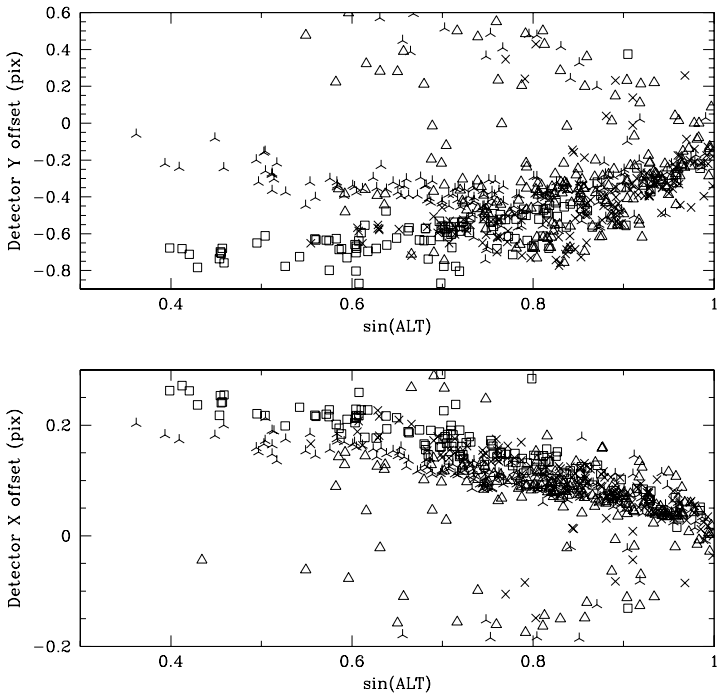

Figure 5. The same plots as figure 4 except that *only* parameters X_d and Y_d were open during optimisation. Note here both the correlation with sin ALT and with POSANG (symbols as figure 4).

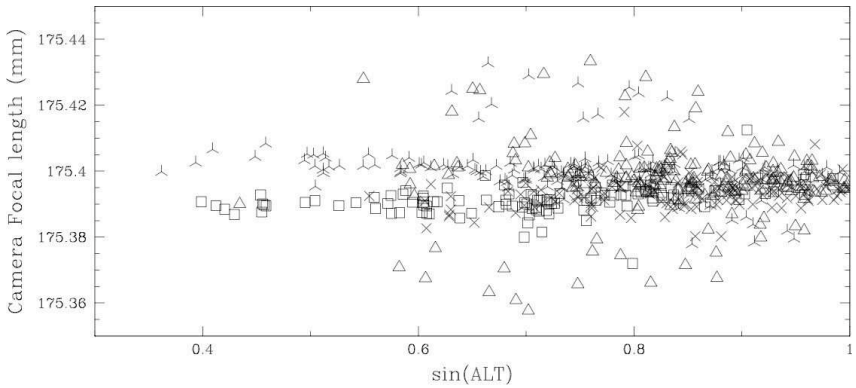

Figure 6. The optimal value of the NIR camera focal distance parameter, f_d, determined via application of the optimisation process with XSPM parameters τ_d, f_d, μ_g and ν_g open, plotted against the sin of the ALT header keyword. POSANG values are represented by symbols as in figure 4.

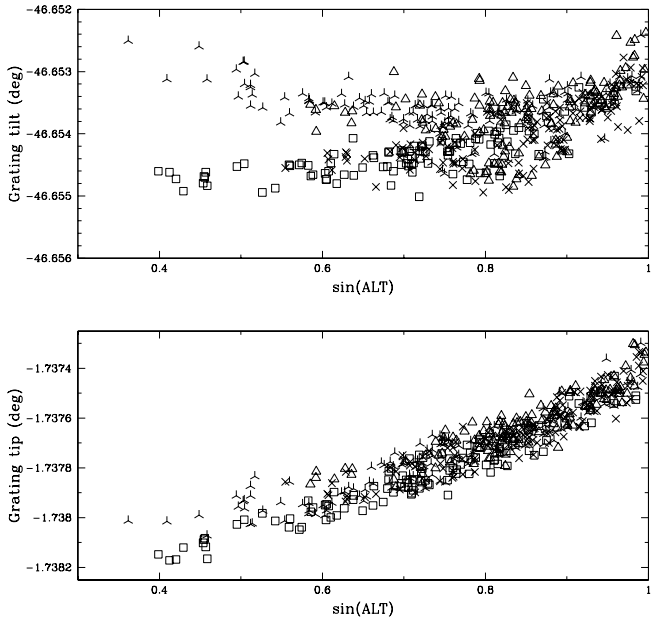

Figure 7. **Top:** The optimal value of the NIR grating tilt parameter, μ_g, determined via application of the optimisation process with XSPM parameters τ_d, f_d, μ_g and ν_g open, plotted against the sin of the ALT header keyword. POSANG values are represented by symbols as in figure 4. **Bottom:** The same plot for the NIR grating tip parameter, ν_g.

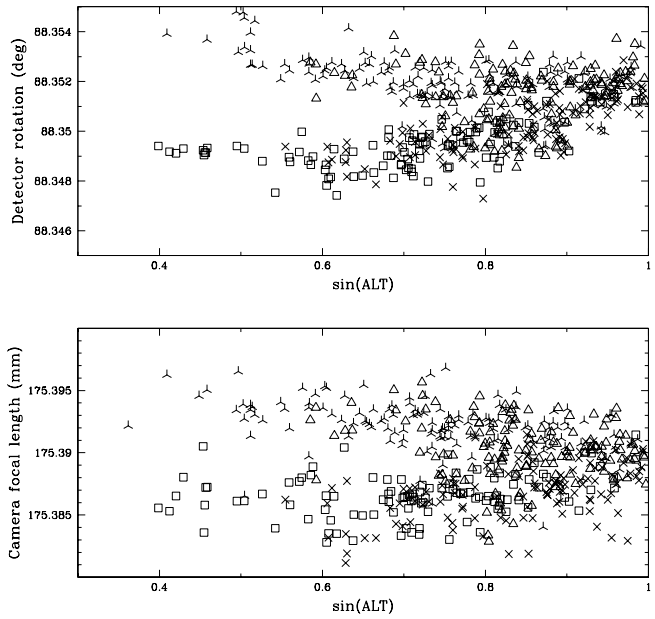

Figure 8. **Top:** The optimal value of the NIR camera focal distance, f_d, determined via application of the optimisation process with XSPM parameters τ_d, f_d, μ_g and ν_g open, plotted against the sin of the ALT header keyword. POSANG values are represented by symbols as in figure 4. **Bottom:** The same plot for the NIR detector rotation parameter, τ_d.

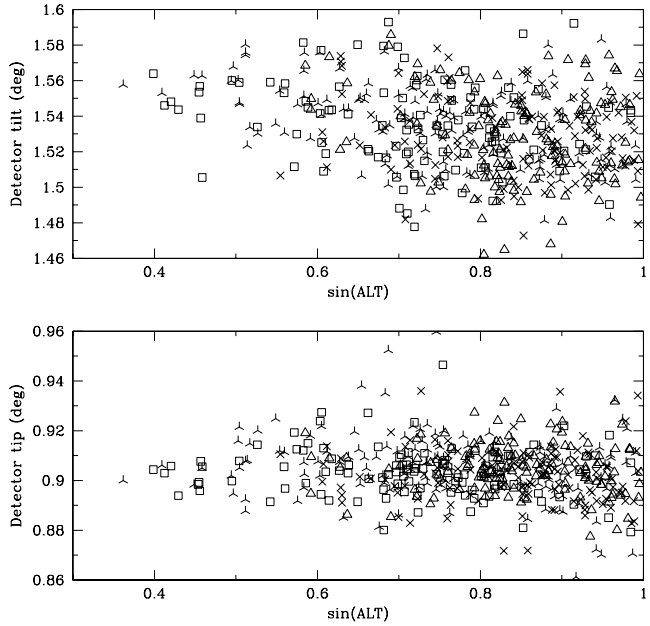

Figure 9. **Top:** The optimal value of the NIR detector tilt parameter, μ_d, determined via application of the optimisation process with XSPM parameters τ_d, f_d, μ_g, ν_g, μ_d and ν_d open, plotted against the sin of the ALT header keyword. POSANG values are represented by symbols as in figure 4. **Bottom:** The same plot for the NIR detector tip parameter, ν_d.

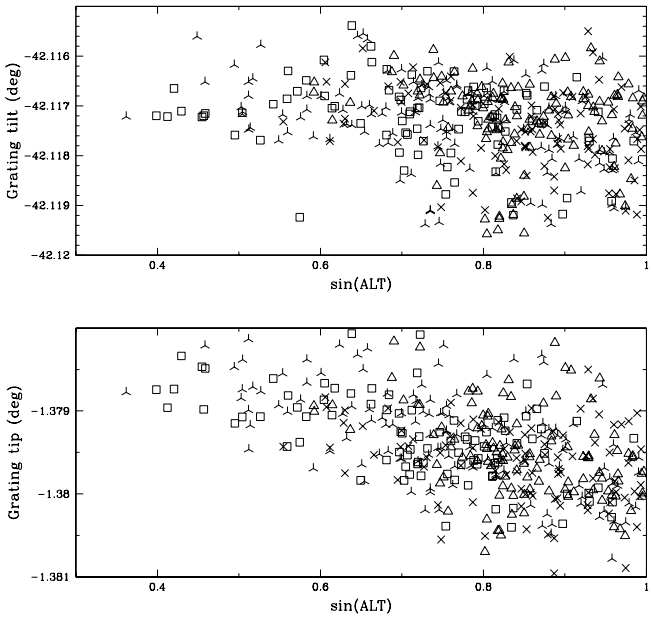

Figure 10. **Top:** The optimal value of the UVB grating tilt parameter, μ_g, determined via application of the optimisation process with XSPM parameters τ_d, f_d, μ_g and ν_g open, plotted against the sin of the ALT header keyword. POSANG values are represented by symbols as in figure 4. **Bottom:** The same plot for the UVB grating tip parameter, ν_g.

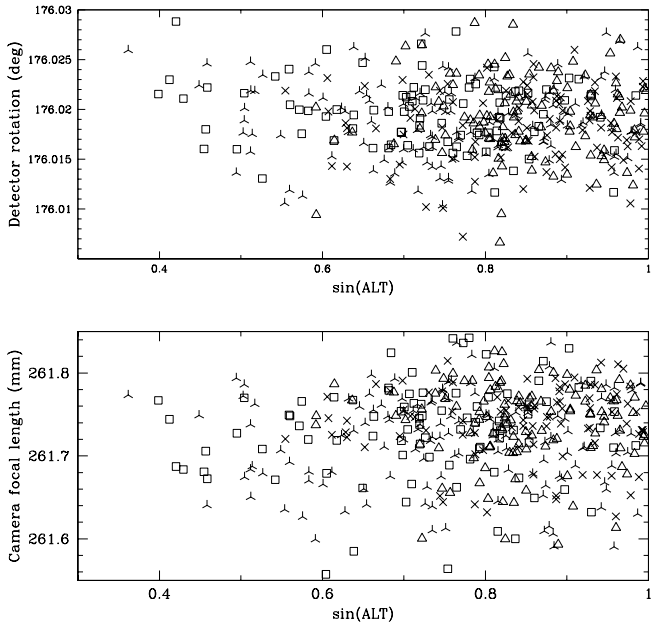

Figure 11. **Top:** The optimal value of the UVB camera focal distance, f_d, determined via application of the optimisation process with XSPM parameters τ_d, f_d, μ_g and ν_g open, plotted against the sin of the ALT header keyword. POSANG values are represented by symbols as in figure 4. **Bottom:** The same plot for the UVB detector rotation parameter, τ_d.

Acknowledgements

It is a pleasure to thank all members of the X-shooter team for useful collaboration. In particular Paolo Goldoni, Regis Haigron and Frederic Royer have helped us tremendously in integrating the physical model into the DRS.

REFERENCES

[1] D'Odorico S. et al. 2006, SPIE, 6269, 626933

[2] P. Spano' et al, "X-shooter Optical Design Report", ESO internal document **XSH-TRE-ITA-2700-0027** Issue 2.1 (2006)

[3] Modigliani, A. et al. 2010, SPIE, 7737-85, "The X-shooter pipeline."

[4] P. Bristow, F. Kerber, M. R. Rosa, "Advanced Calibration Techniques for Astronomical Spectrographs", The Messenger, **131**, p2 (2008)

[5] Bristow, P. et al. 2008, SPIE, Volume 7014, pp. 70143X-70143X-9

[6] Moehler, S. et al. 2010, SPIE, 7737-56

[7] Kirkpatrick, S., C.D. Gelatt Jr, and M.P. Vecchi; "Optimization by Simulated Annealing", *Science*, **220, No. 4598**, 671 - 680 (1983)

[8] Press, W.H., B.P. Flannery, S.A. Teukolsky and W.T. Vetterling; [Numerical Recipes, The Art of Scientific Computing], Cambridge Univ. Press, Cambridge, UK (1986)

[9] P. Ballester, M. R. Rosa, "Modelling echelle spectrographs", *A&AS* **126**, 563–571 (1997)

[10] Carter E., http://www.taygeta.com/annealing/simanneal.html (2001)

[11] Mazzoleni, R. et al. 2005 "Automatic Flexure Compensation System"

[12] Dekker, H. & Mazzoleni, R. 2005 "X-shooter Flexure Compensation System", ESO internal document **XSH-TRE-ESO-2000-0100**